Solar Energy 145 (2017) 27–32

Contents lists available at ScienceDirect

Solar Energy

journal homepage: www.elsevier.com/locate/solener

Fabrication of Cu_2SnS_3 thin film solar cells using Cu/Sn layered metallic precursors prepared by a sputtering process

Ju Yeon Lee [a], In Young Kim [b], Mahesh P. Surywanshi [a], Uma V. Ghorpade [a,c], Dong Seon Lee [b], Jin Hyeok Kim [a,*]

[a] Optoelectronics Convergence Research Center, Department of Material Science and Engineering, Chonnam National University, 300 Yongbong-Dong, Buk-Gu, Gwangju 500-757, South Korea
[b] School of Information and Communications, Gwangju Institute of Science and Technology, 123 Cheomdangwagi-ro, Buk-gu, Gwangju 500-712, South Korea
[c] Analytical Chemistry and Material Science Research Laboratory, Department of Chemistry, Shivaji University, Kolhapur 416 004, India

ARTICLE INFO

Article history:
Received 15 March 2016
Received in revised form 8 September 2016
Accepted 28 September 2016
Available online 13 October 2016

Keywords:
Cu_2SnS_3
Thin film solar cells (TFSCs)
Sputtering method
Raman

ABSTRACT

As an alternative to $Cu(In,Ga)(S,Se)_2$ (CIGS) and $Cu_2ZnSn(S,Se)_4$ (CZTS)-based thin film solar cells (TFSCs), the ternary chalcogenide semiconductor Cu_2SnS_3 (CTS) is an emerging material with suitable optical band gap energy ranging from 0.93 to 1.77 eV and high absorption coefficients ($>10^4$ cm^{-1}). In this study, we report the preparation of high-quality CTS thin films by the annealing of the sputtered Cu-Sn metallic precursor under S vapor atmosphere in a graphite box using the RTA process. Furthermore, the influence of different S vapor partial pressures in the graphite box during annealing on the properties of the CTS thin films has been investigated systematically. It is observed that the properties and photovoltaic performance of the CTS thin films are strongly dependent on the S vapor partial pressure during annealing. The monoclinic crystal structure is observed from X-ray diffraction (XRD) of the (1 1 2), (2 2 0), and (3 1 2) planes, and it is further confirmed using Raman spectroscopy by the presence of Raman peaks at 295 and 354 cm^{-1}. The direct band gap energy is found to be 0.91 eV by extrapolation from external quantum efficiency (EQE) measurement of a CTS thin film annealed using 60 mg of S powder. The preliminary best power conversion efficiency (PCE) of 2.21% with a short circuit current density of 29.7 mA/cm^2, an open circuit voltage of 179.5 mV, and a fill factor of 41% have been obtained for a CTS thin film annealed using 60 mg of S powder, although the processing parameters have not been optimized.

1. Introduction

$Cu(In,Ga)(S,Se)_2$ (CIGS)-based thin film based solar cells (TFSCs) have received notable attention because of their high optical absorption coefficient ($\sim 10^4$ cm^{-1}) and wide range of direct-band gap energy (1.0–1.6 eV) (Jackson et al., 2012; Chirilă et al., 2013). The cells' high optical absorption that enables a low absorber thickness ($\sim$1 μm) to effectively capture sufficient sunlight is another advantage that makes them appropriate for commercial use. Since the highest efficiency measurement of higher than 20% was reported (Jackson et al., 2014; Dhakal et al., 2013), studies of CIGS TFSC technology have become popular, providing the potential for next-generation commercial TFSCs over Si-based TFSCs. However, CIGS-based TFSCs are challenged by several issues such as its toxic and rare-earth constituent elements and the difficulty of controlling a secondary phase formation during the annealing process (Ghorpade et al., 2014; Suryawanshi et al., 2013; Krustok et al., 2010).

To overcome the detrimental issues associated with existing TFSC materials, the Cu_2SnS_3 (CTS) semiconductor has received considerable attention as a suitable candidate for TFSCs due to its high optical absorption coefficient ($\sim 10^4$ cm^{-1}) and theoretical power conversion efficiency (PCE, 33%) (Kotaro et al., 2012; Lokhande et al., 2016). Moreover, CTS exhibits a wider range of band gap energy (0.9–1.7 eV) than existing TFSC materials, and it is relatively easy to control the secondary phase formation compared to quaternary compounds. It is also well known that CTS exhibits a variety of crystal structures such as cubic, tetragonal, monoclinic, and orthorhombic, which are strongly dependent on the preparation method and annealing conditions (Mitsuki et al., 2015; Ayaka et al., 2015). Therefore, it is very important to precisely choose the preparation method and optimize the working and annealing conditions to obtain the desired crystal structure with the desired composition and optical band gap energy.

* Corresponding author.
E-mail address: jinhyeok@chonnam.ac.kr (J.H. Kim).

http://dx.doi.org/10.1016/j.solener.2016.09.041
0038-092X/

Recently, a record PCE of 4.63% has been achieved for CTS TFSCs fabricated using the evaporation method, proving its potential for next-generation TFSCs (Mitsuki et al., 2015). In spite of its higher efficiency, CTS thin films fabricated by the evaporation technique suffer from a lack of uniformity and compositional controllability (Mitsuki et al., 2015). As an alternative to the evaporation method, sputtering is an appropriate approach to overcome these issues and fabricate high-quality CTS thin films. Using the sputtering method, it is possible to deposit high-quality thin films with good reproducibility using a simple process. In addition, materials with a high melting point can be easily deposited with the desired thickness using the sputtering process (Kanai et al., 2015). However, the sputtering method for preparing CTS thin films has been sparsely studied, and the reported works are limited to the preparation of these thin films.

Here, we report the preparation of high-quality CTS thin films by annealing the sputtered Cu/Sn metallic precursor in an S vapor atmosphere in a graphite box using the RTA process. The amount of S powder used during the annealing is one of the key parameters in the preparation of high-quality CTS thin films, as it relates to the S vapor partial pressure inside the graphite box, which significantly affects the grain growth and secondary phase formation. Therefore, we also explored the effect of the amount of S powder on the properties and photovoltaic performance of CTS TFSCs. The crystallographic, morphological, and compositional properties and photovoltaic performance were systematically analyzed to define the crystal structure in detail and prove the effectiveness of the CTS-based TFSCs prepared by the sputtering process. In particular, we demonstrated a notable efficiency of 2.21% by optimizing the amount of S powder used during annealing.

Table 1
The partial pressure of sulfur according to the amount of sulfur powder in graphite box.

Sample	Quantity of S powder (mg)	Pressure inside graphite box (kPa)
CTS3	30	133.2
CTS6	60	266.3
CTS9	90	399.5

Table 2
List of the interfacial MoS_2 thickness measured by FE-SEM.

Sample	Thickness of MoS_2 (nm)
CTS3	71
CTS6	94
CTS9	109

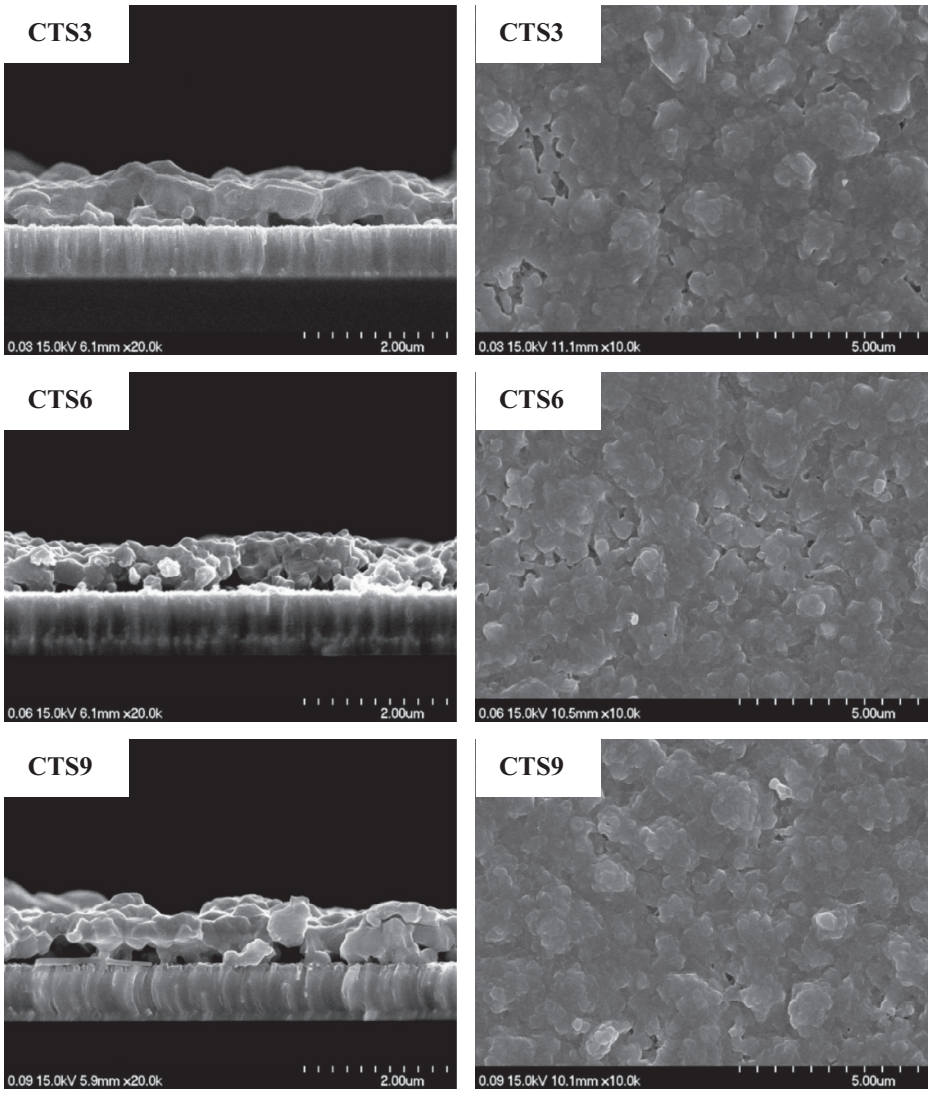

Fig. 1. The surface and cross sectional FE-SEM images of CTS thin films annealed using different amount of S powder.

2. Experimental details

Precursor films were deposited on molybdenum (Mo)-coated soda lime glass (SLG) substrates using a magnetron sputtering system equipped with two 4-inch magnetron cathodes (Cu and Sn). Elemental targets (Cu: 5 N purity, Sn: 5 N purity) were used for the depositions of precursor films. The depositions were carried out under a sputtering power of 30 W and a process pressure of 8 mTorr. The depositions of the Cu and Sn metallic layers were conducted for 35 and 45 min, respectively. The precursor films were annealed at 580 °C for 10 min in an S vapor atmosphere using a tube-type RTA process. The temperature was increased from room temperature to 580 °C at a rate of 10 °C/s, and subsequently held for 10 min. The amount of S powder was varied among 30, 60, and 90 mg (sulfur: reagent grade, powder, purified by refining-100 mesh particle size). Table 1 shows the corresponding S partial pressure by amount of S powder in graphite box. Hereafter, the annealed films are denoted as CTS3, CTS6 and CTS 9, respectively.

The annealed CTS thin films were used to fabricate photovoltaic cells with the structure of SLG/Mo/CTS-absorber/CdS/i-ZnO/ZnO:Al/Al. The deposition of a cadmium sulfide (CdS) buffer layer was performed using the chemical bath deposition method, and i-ZnO and Al-doped ZnO window layers were deposited using the sputtering method. The aluminum front grid was formed using a direct current (DC) sputtering process.

The surface and cross-sectional morphologies were observed using field emission scanning electron microscopy (FE-SEM, JSM-6701F, JEOL, Japan). The crystal structure of the CTS thin film was examined using high-resolution X-ray diffraction (XRD, X'pert PRO, Philips, Eindhoven, Netherlands) operated at 40 kV and 30 mA with Ni-filtered Cu Kα radiation [λ = 1.54056 Å]. Micro Raman spectroscopy (Via Reflex UV Raman microscope, Renishaw, U.K. at KBSI Gwangju Center) at an excitation wavelength of 488 nm and a resolution of 1 cm^{-1} at 15 mW laser power with a He-Ne laser source was used to record Raman spectra in the range of 200–500 cm^{-1}. The binding energy was confirmed by X-ray photoelectron spectroscopy (XPS, VG Multilab 2000, Thermo VG Scientific, U.K.) with a monochromatic Mg Kα (1253.6 eV) radiation source. The binding energy in the spectrometer was calibrated using the C 1s line at 285.0 eV. Compositional studies were conducted using X-ray fluorescence spectroscopy (XRF, ZSX primus II, RIKAKU, Japan). The PCE and quantum efficiency (QE) for CTS TFSCs were characterized using a class AAA solar simulator (Sol31, Oriel, USA) and an incident photon conversion efficiency measurement unit (PV Measurement, Inc., USA), respectively.

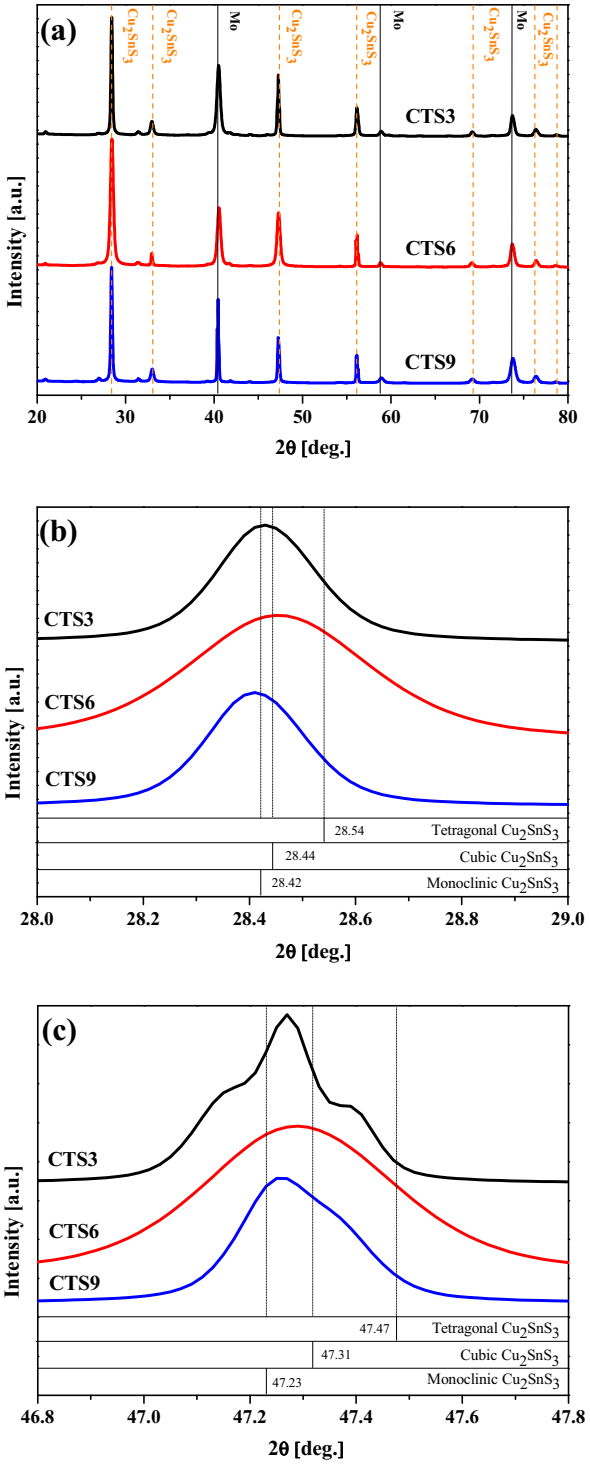

Fig. 2. (a) X-ray diffraction patterns of annealed CTS thin films, (b) enlarged scale of (1 1 2) diffraction plane in XRD spectra of annealed CTS thin films, and (c) enlarged scale of (2 2 0) diffraction plane in XRD spectra of annealed CTS thin films.

3. Results and discussion

Fig. 1 shows the cross-sectional and surface FE-SEM images of CTS thin films annealed using different amounts of S powder at 580 °C for 10 min. All of the annealed films show thicknesses in

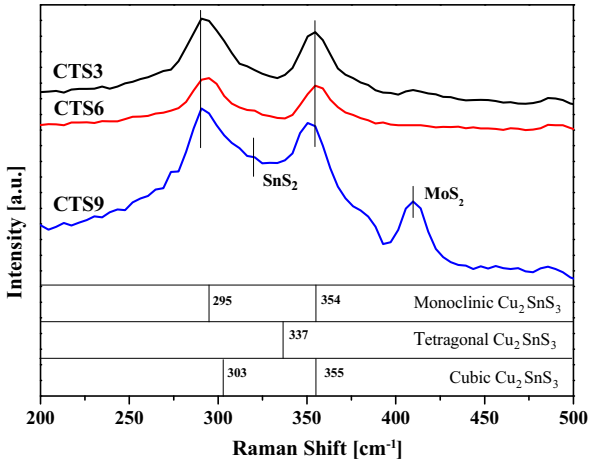

Fig. 3. Raman spectra of CTS thin films annealed using different amount of S powder.

the range of ~800 nm and locally aggregated grains on the overall surface. Although dense and smooth grain growth is observed in the cross-sectional images, holes and voids are locally scattered on the interface between the CTS absorber and the Mo back contact electrode, regardless of the sulfur pressure, which remains an issue. It possibly acts as a shunt path and trapping site that has a detrimental effect on the device while preventing carrier collection (Xie et al., 2013). On the other hand, the formation of a thin layer of MoS_2 (~100 nm) at the interface between the CTS absorber and Mo in the CTS9 sample is observed. The thicknesses of the interfacial MoS_2 for all samples are listed in Table 2. The CTS9 sample also exhibits a relatively rough surface morphology that may build a poor junction with the buffer layer, which significantly affects the device performance (Ghorpade et al., 2015).

Fig. 2 shows the XRD patterns of CTS thin films annealed using different amounts of S powder. All the films exhibit diffraction peaks at $2\theta = 28.42$, 32.97, 47.27, 56.15, 69.17, 76.37, and 78.65°, which correspond to the (1 1 2), (103), (2 2 0), (312), (224), (400), (332), and (420) diffraction planes of monoclinic CTS [JCPDS card No; 89-2877], respectively (Dahman et al., 2014; Tiwari et al., 2013). The intensity of the peak intense diffraction peak along the (1 1 2) plane is negligibly affected by the S vapor partial pressure inside the graphite box. Upon enlarging the scale of the (1 1 2) and (2 2 0) diffraction peaks, the slightly different position of the peaks is observed, as shown in Fig. 2(b) and (c). It is observed that the peak positions in the CTS3 and CTS9 samples are closer to monoclinic, whereas they are slightly closer to a tetragonal structure in the CTS6 sample. In the CTS3 sample, extra peaks of secondary phases such as SnS (JCPDS card no. 89-2755) and Cu_8S_5 (JCPDS card no. 33-0491) are scattered around the (2 2 0) diffraction peak, whereas no traces of any secondary phases are observed in the CTS6 and CTS 9 samples.

It is difficult to detect what type of crystal structure is formed in the annealed CTS thin films using XRD patterns alone because of the similar peak positioning (Fernandes et al., 2010). Therefore, Raman analysis was employed to confirm the crystal structure

Table 3
Elemental compositions and compositional ratios of the sulfurized films determined by XRF.

Sample	Cu (at.%)	Sn (at.%)	S (at.%)	Cu/Sn	S/M
CTS3	0.278	0.195	0.528	1.425	1.117
CTS6	0.271	0.200	0.529	1.353	1.121
CTS9	0.269	0.196	0.534	1.373	1.148

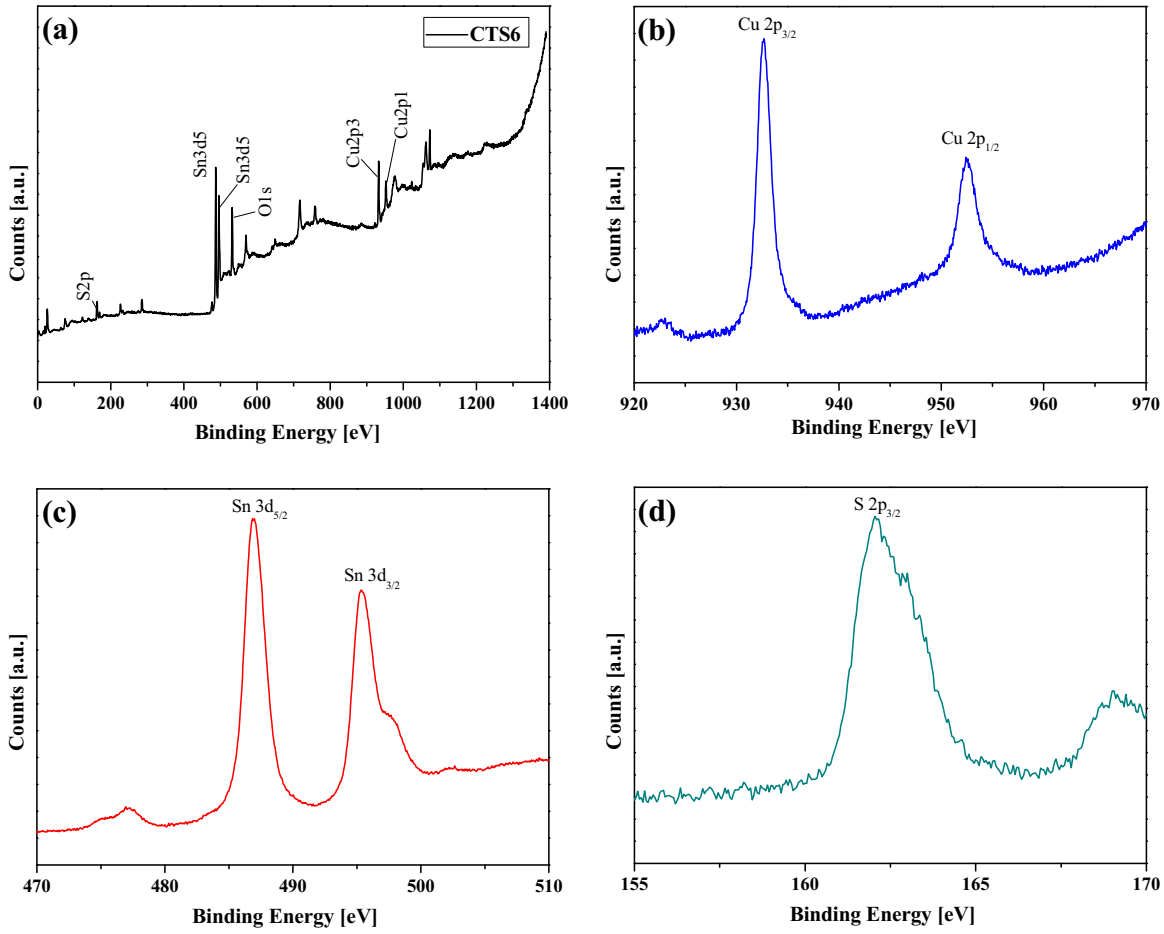

Fig. 4. XPS spectrum of CTS thin films sulfurized using 60 mg of S powder. (a) typical survey spectrum, (b) Cu 2p core level, (c) Sn 3d core level, and (d) S 2p core level.

and secondary phase formation in CTS thin films. Fig. 3 shows the Raman spectra of a CTS thin film annealed using different amounts of S powder. Two dominant peaks at 295 and 354 cm^{-1} corresponding to the CTS monoclinic phase are observed in all CTS samples (Berg et al., 2012). The CTS9 sample exhibits the presence of an extra peak at 318 cm^{-1}, attributed to the formation of a secondary phase of SnS_2 (Mathews et al., 2013). In addition, the formation of MoS_2 that is observed in the cross-sectional FE-SEM image is confirmed by the presence of a Raman peak at 405 cm^{-1} in the CTS9 sample (Lund et al., 2014; Kibsgaard et al., 2012; Emrani et al., 2013).

Table 3 shows the elemental compositions and compositional ratios of the CTS samples annealed using different amounts of sulfur powder measured using XRF spectroscopy. All the films show considerably Cu-poor compositions, irrespective of the S quantity, and the S/metal ratio is higher than unity. Furthermore, to confirm the valence states of Cu, Sn and S, the CTS6 sample was analyzed by XPS, as shown in Fig. 4, which presents the core level photoelectron spectra of Cu, Sn, and S including carbon and oxygen in the full XPS spectrum. The presence of carbon and oxygen impurities in the core level spectrum is due to exposure of the samples to the atmosphere. The binding energy peaks of Cu $2p_{1/2}$ and Cu $2p_{3/2}$ appear at 952.5 and 932.6 eV, respectively, which indicates that Cu is present in its Cu^+ state. It also shows the binding energy of Sn $3d_{5/2}$ and Sn $3d_{3/2}$ at 495.5 and 486.9 eV, respectively, providing evidence for the existence of the Sn^{4+} ionic state. The 2p peaks of S are observed at 162.4 eV, implying the existence of S in its sulfide states (Cahen et al., 1985; Partain et al., 1985).

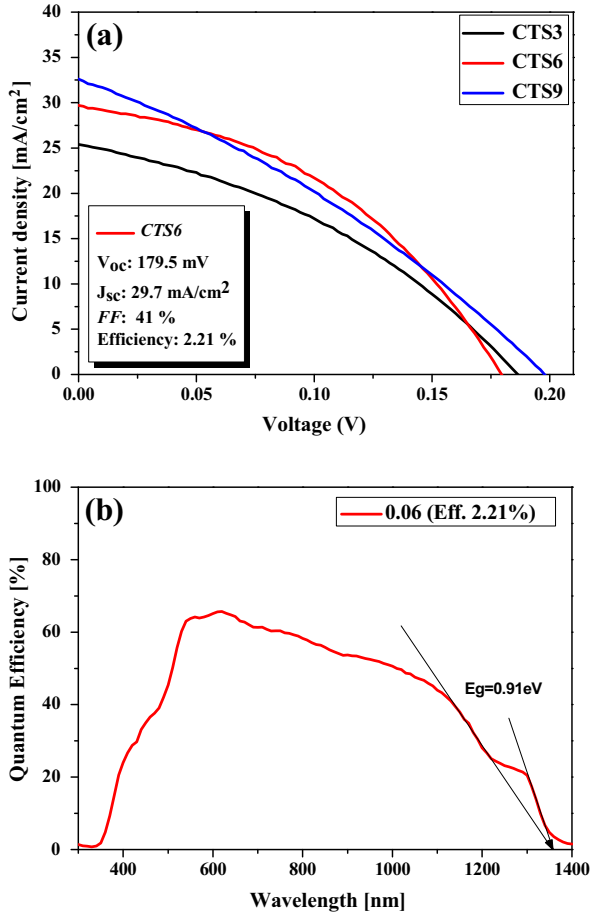

Fig. 5. Photovoltaic properties of CTS3, CTS6, and CTS9 devices annealed using different amount of S powder (a) J-V characteristics and (b) external quantum efficiency (EQE) spectrum of CTS6 sample.

To investigate the effectiveness of our sputtering method, CTS thin films annealed using different amounts of S were processed into TFSCs. Fig. 5(a) shows the current density-voltage (J-V) characteristics under AM 1.5 G illumination of CTS devices. The detailed device parameters are listed in Table 4. The CTS device fabricated using the CTS6 sample annealed using 60 mg of S powder showed the highest PCE of 2.21%, with an open circuit voltage (V_{oc}) of 179.5 mV, short circuit current density (J_{sc}) of 29.7 mA/cm^2, and fill factor (FF) of 41%. Despite the CTS9 device having the highest V_{oc} of 197.7 mV and J_{sc} of 32.6 mA/cm^2 among all the CTS devices, its efficiency is lower than that of the CTS6 device because of its relatively low FF of 32. In the crystallographic analysis, the CTS9 sample shows the existence of secondary phases and the formation of a MoS_2 layer at the interface between the CTS absorber and Mo substrates, which might affect the FF, thereby lowering the device performance (Scragg et al., 2012). On the other hand, the presence of secondary phases of SnS and Cu_8S_5 in the CTS3 sample, as confirmed from XRD results, may attenuate the visible light absorption, resulting in the lowest efficiency among all the samples. The highest efficiency of 2.21% in the CTS6 device is attributed to the formation of pure phase CTS and a uniform microstructure, which contributes to the formation of a homogeneous junction between the absorber and buffer layer. These factors increase the FF of the CTS solar device (Cao et al., 2013). In addition, CTS6 has the lowest sheet resistance (R_s) of 8.2 Ω/cm^2 and the highest shunt resistance (R_{sh}) of 111.1 Ω/cm^2. The low R_{sh} is an important factor that implies the shunt path leading to the recombination of charge carriers at deep traps in the band gap, which suggests the form of an incomplete p-n junction that leads to extensive recombination at the buffer/absorber interface (Chen et al., 2012). EQE measurements were carried out for the highest efficiency CTS 6 device, as shown in Fig. 5(b). The gradual decrease in the EQE value in the long-wavelength region gives the quality of the CTS absorber layer. The highest value of quantum efficiency of ~63% is achieved for the CTS6 device. The gradual decrease in the EQE at longer wavelengths may result from the loss of absorbed photons due to the short minority carrier life-time in the absorber layers (Scragg et al., 2010).

Although, the efficiency of 2.21% achieved for CTS thin films prepared using the sputtering method, it is relatively low compared with the record conversion efficiency of 4.63%. Several investigations such as on precise composition control and optimization of annealing conditions are in progress in our laboratory.

Table 4
Photovoltaic parameters of the Cu_2SnS_3 TFSCs evaluated from the solar simulator.

Sample	V_{oc} (mV)	J_{sc} (mA/cm^2)	Eff. (%)	*FF* (%)	R_s (Ω/cm^2)	R_{sh} (Ω/cm^2)
CTS3	186.5	25.4	1.74	37	12.1	100.0
CTS6	179.5	29.7	2.21	41	8.2	111.1
CTS9	197.7	32.6	2.04	32	11.0	47.6

4. Conclusions

CTS thin films have been successfully prepared using the sputtering method. The effect of sulfur quantity corresponding to the annealing partial pressure on the crystallographic, morphological, and compositional properties and photovoltaic performance of CTS thin films is investigated. The formation of pure phase CTS with monoclinic structure, uniform microstructure and compositional anisotropy is observed in the optimized CTS thin film annealed using 60 mg of S powder. The presence of all elements in their respective ionic states of Cu^{1+}, Sn^{4+}, and S^{2-} was confirmed from XPS for the optimized CTS thin film. The band gap energy is found to be 0.91 eV from the extrapolation of EQE spectra. The device fabricated using the optimized CTS thin film exhibited the highest efficiency of 2.21% with V_{oc} of 179.5 mV, J_{sc} of 29.7 mA/cm^2, and FF of 41%.

Acknowledgment

This work was supported by the Human Resources Development program (No. 20124010203180) of the Korea Institute of Energy Technology Evaluation and Planning (KETEP) grant funded by the Korea government Ministry of Trade, Industry and Energy. The National Research Foundation of Korea (NRF) funded by the Ministry of Science, ICT & Future Planning (NRF-2015R1A2A2A01006856).

References

Ayaka, K., Kotoba, T., Kotaro, C., Hironori, K., Hideaki, A., 2015. Fabrication of Cu_2SnS_3 thin- film solar cells with power conversion efficiency of over 4%. Jpn. J. Appl. Phys. 54, 08KC06.

Berg, D.M., Djemour, R., Gütay, L., Siebentritt, S., Dale, P.J., Fontane, X., Izquierdo-Roca, V., Pérez-Rodriguez, A., 2012. Raman analysis of monoclinic Cu_2SnS_3 thin films. Appl. Phys. Lett. 100, 192103.

Cahen, David, Ireland, P.J., Kazmerski, L.L., Thiel, F.A., 1985. X-ray photoelectron and Auger electron spectroscopic analysis of surface treatments and electrochemical decomposition of copper indium selenide ($CuInSe_2$) photoelectrodes. J. Appl. Phys. 57, 4761.

Cao, M., Li, L., Zhang, B.L., Huang, J., Wang, L.J., Shen, Y., Sun, Y., Jiang, J.C., Hu, G.J., 2013. One-step deposition of Cu_2ZnSnS_4 thin films for solar cells. Sol. Energy Mater. Sol. Cells 117, 81–86.

Chen, Q., Dou, X., Ni, Y., Cheng, S., Zhuang, S., 2012. Study and enhance the photovoltaic properties of narrow-bandgap Cu_2SnS_3 solar cell by p-n junction interface modification. J. Colloid Interface Sci. 376, 327–330.

Chirilă, A., Reinhard, P., Pianezzi, F., Bloesch, P., Uhl, A.R., Fella, C., Kranz, L., Keller, D., Gretener, C., Hagendorfer, H., Jaeger, D., Erni, R., Nishiwaki, S., Buecheler, S., Tiwari, A.N., 2013. Potassium-induced surface modification of Cu(In, Ga)Se_2 thin films for high-efficiency solar cells. Nat. Mater. 12, 1107–1111.

Dahman, H., Rabaoui, S., Alyamani, A., El Mir, L., 2014. Structural, morphological and optical properties of Cu_2SnS_3 thin film synthesized by spin coating technique. Vacuum 101, 208–211.

Dhakal, T., Peng, C., Tobias, R.R., Dasharathy, R., Westgate, C., 2013. Characterization of a CZTS thin film solar cell grown by sputtering method. Sol. Energy 100, 23–30.

Emrani, A., Vasekar, P., Westgate, C., 2013. Effects of sulfurization temperature on CZTS thin film solar cell performances. Sol. Energy 98, 335–340.

Fernandes, P.A., Salomé, P.M.P., da Cunha, A.F., 2010. Cu_xSnS_{x+1} (x = 2, 3) thin films grown by sulfurization of metallic precursors deposited by dc magnetron sputtering. Phys. Status Solidi C 7, 901–904.

Ghorpade, U., Suryawanshi, M., Shin, S.W., Gurav, K., Patil, P., Pawar, S., Hong, C.W., Kim, J.H., Kolekar, S.S., 2014. Towards environmentally benign approaches for the synthesis of CZTSSe nanocrystals by a hot injection method: a status review. Chem. Commun. 50, 11258–11273.

Ghorpade, U.V., Suryawanshi, M.P., Shin, S.W., Hong, C.W., Kim, I.Y., Moon, J.H., Yun, J.H., Kim, J.H., Kolekar, S.S., 2015. Wurtzite CZTS nanocrystlas and phase evolution to kesterite thin film for solar energy harvesting. Phys. Chem. Chem. Phys. 17, 19777–19788.

Jackson, P., Hariskos, D., Lotter, E., Paetel, S., Wuerz, R., Menner, R., Wischmann, W., Powalla, M., 2012. New world record efficiency for Cu(In,Ga)Se_2 thin-film solar cells beyond 20%. Prog. Photovolt.: Res. Appl. 19, 894–897.

Jackson, P., Hariskos, D., Würz, R., Wischmann, W., Powalla, M., 2014. Compositional investigation of potassium doped Cu(In, Ga)Se_2 solar cells with efficiencies up to 20.8%. Phys. Status Solidi RRL 8, 219–222.

Kanai, A., Araki, H., Takeuchi, A., Katagiri, H., 2015. Annealing temperature dependence of photovoltaic properties of solar cells containing Cu_2SnS_3 thin films produced by co-evaporation. Phys. Status Solidi B 252, 1239–1243.

Kibsgaard, J., Chen, Z., Benjamin, N.R., Jaramillo, T.F., 2012. Engineering the surface structure of MoS_2 to preferentially expose active edge sites for electrocatalysis. Nat. Mater. 11, 963–969.

Kotaro, C., Junpei, K., Shinya, E., Hideaki, A., Ryota, N., Kazuo, J., Hironori, K., 2012. Preparation of Cu_2SnS_3 thin films by sulfurization of Cu/Sn stacked precursors. Jpn. J. Appl. Phys. 51, 10NC35.

Krustok, J., Josepson, R., Danilson, M., Meissner, D., 2010. Temperature dependence of $Cu_2ZnSn(Se_xS_{1-x})_4$ monograin solar cells. Sol. Energy 84, 379–383.

Lokhande, A.C., Gurav, K.V., Jo, E., Lokhande, C.D., Kim, J.H., 2016. Chemical synthesis of Cu_2SnS_3 (CTS) nanoparticles: a status review. J. Alloys Compd. 656, 295–310.

Lund, E.A., Du, H., Hlaing, W.M., Teeter, G., Scarpulla, M.A., 2014. Investigation of combinatorial coevaporated thin film Cu_2ZnSnS_4 (II): beneficial cation arrangement in Cu-rich growth. J. Appl. Phys. 115, 173503-1–173503-11.

Mathews, N.R., Tamy Benítez, J., Paraguay-Delgado, F., Pal, M., Huerta, L., 2013. Formation of Cu_2SnS_3 thin film by the heat treatment of electrodeposited SnS–Cu layers. J. Mater. Sci.: Mater. Electron. 24, 4060–4067.

Mitsuki, N., Junya, F., Toshiyuki, Y., Masanobu, I., 2015. Cu_2SnS_3 thin-film solar cells fabricated by sulfurization from NaF/Cu/Sn stacked precursor. Appl. Phys. Express 8, 042303.

Mitsuki, N., Junya, F., Toshiyuki, Y., Masanobu, I., 2015. Cu_2SnS_3 thin- film solar cells fabricated by sulfurization from NaF/Cu/Sn stacked precursor. Appl. Phys. Express 88, 042303.

Partain, L.D., Schneider, R.A., Donaghey, L.F., McLeod, P.S., 1985. Surface chemistry of Cu_xS and Cu_xS/CdS determined from X-ray photoelectron spectroscopy. J. Appl. Phys. 57, 5056–5065.

Scragg, J.J., Berg, D.M., Dale, P.J., 2010. A 3.2% efficient kesterite device from electrodeposited stacked elemental layer. J. Electroanal. Chem. 646, 52–59.

Scragg, J.J., Watjen, J.T., Edoff, M., Ericson, T., Kubart, T., Bjorkman, C.P., 2012. A detrimental reaction at the molybdenum back contact in $Cu_2ZnSn(S, Se)_4$ thin-film solar cells. J. Am. Chem. Soc. 134, 19330–19333.

Suryawanshi, M.P., Agawane, G.L., Bhosale, S.M., Shin, S.W., Patil, P.S., Kim, J.H., Moholkar, A.V., 2013. CZTS based thin film solar cells: a status review. Mater. Technol. 28, 98–109.

Tiwari, D., Chaudhuri, T.K., Shripathi, T., Deshpande, U., Rawat, R., 2013. Non-toxic, earth-abundant 2% efficient Cu_2SnS_3 solar cell based on tetragonal films direct-coated from single metal–organic precursor solution. Sol. Energy Mater. Sol. Cells 113, 165–170.

Xie, M., Zhuang, D., Zhao, M., Zhuang, Z., Ouyang, L., Li, X., Song, J., 2013. Preparation and characterization of Cu_2ZnSnS_4 thin films and solar cells fabricated from quaternary Cu–Zn–Sn–S target. Int. J. Photoenergy, 9.